# Two-component self-assemblies: investigation of a synergy between bis-urea stickers

Emilie Ressouche, Sandrine Pensec, Benjamin Isare, Jacques Jestin, Laurent Bouteiller

# Two-component self-assemblies: investigation of a synergy between bis-urea stickers

*Emilie Ressouche,† Sandrine Pensec,† Benjamin Isare,† Jacques Jestin,‡ and Laurent Bouteiller*†*

† Sorbonne Universités, UPMC Univ Paris 06, CNRS, Institut Parisien de Chimie Moléculaire, Equipe Chimie des Polymères, 4 Place Jussieu, F-75005 Paris, France

‡ Laboratoire Léon Brillouin, UMR 12 CNRS-CEA, 91191 Gif-sur-Yvette Cedex, France

ABSTRACT. It is of interest to develop two-component systems for added flexibility in the design of supramolecular polymers, nanofibers or organogels. Bis-ureas are known to self-assemble by hydrogen bonding into long supramolecular objects. We show here that mixing aromatic bis-ureas with slightly different structures can yield surprisingly large synergistic effects. A strong increase in viscosity is observed when a bis-urea with the sterically demanding 2,4,6-trimethylbenzene spacer is combined with a bis-urea bearing no methyl group in position 2 of the aromatic spacer (i.e. 4-methylbenzene or 4,6-dimethylbenzene). This effect is the consequence of a change in supramolecular assembly triggered by the composition of the mixture. The mixture of complementary bis-ureas forms rod-like objects that are more stable by about 1 kJ/mol, and that are thicker than the rod-like objects formed by both parent systems.

## Introduction

Self-assembly of small molecules into large objects of various topologies is of interest in many fields. For instance, self-assembled 1D objects (supramolecular polymers,[1,2] nanofibers,[3] organogels[4,5]) are often developed for their rheological properties or as templates in material science. On surfaces, self-assembled monolayers allow to create functional nanosystems with implications for surface chirality, nanoporous surfaces, optoelectronics or surface reactivity.[6,7,8] Control of the self-assembly process in 3D can lead to composite crystals[9] or to porous frameworks.[10,11,12] While some of these systems may involve a single component bearing a self-complementary sticker that is designed to self-assemble into large objects, it is clearly of interest to develop two-component systems for added flexibility in the design of the properties and to be able to trigger the assembly at will.[13,14] Usually the complementarity between stickers is obvious from their molecular structure, as in the case of metal/ligand,[15,16] host/guest,[17,18] acid/base,[19,20] donor/acceptor[21,22] or complementary hydrogen bonded[23,24,25,26] systems. In contrast, we previously reported the fact that bis-ureas **T** and **M** (Figure 1) form 1D hydrogen bonded co-assemblies that are more stable than each homo-assembly.[27] In this case, the origin of the complementarity between the stickers is not obvious because they are both composed of the same urea moieties, but we actually showed that the complementarity results from subtle steric effects (see below).[27] We recently employed these complementary bis-urea stickers for the rational design of two-component gels,[28] and the aim of the present manuscript is to characterize in detail the structure and the stability of these co-assemblies.

## Experimental Section

**Synthesis.** The synthesis of **T**,[29] **M**,[27] **X**,[30] $\mathbf{T_{PIB}}$,[31] and $\mathbf{X_{PIB}}$[28] was previously reported. The synthesis and the characterization of $\mathbf{M_{PIB}}$ are reported in Supporting Information.

**Viscosimetry.** Measurements were performed with an Anton Paar AMVn falling ball microviscosimeter with a 0.16 mm Ø capillary, with 3 measurements at an angle of +20° and -20°. Results are reported as an average of those 6 measurements.

**Small-angle neutron scattering.** Small-angle neutron scattering measurements were made at the LLB (Saclay, France) on the Pace instrument, at two distance-wavelength combinations to cover the 4 $10^{-3}$ to 0.24 $Å^{-1}$ q-range, where the scattering vector q is defined as usual, assuming elastic scattering ($q=(4\pi/\lambda)\sin(\theta/2)$, where $\theta$ is the angle between incident and scattered beam). Data were corrected for the empty cell signal and the solute and solvent incoherent background. A light water standard was used to normalize the scattered intensities to $cm^{-1}$ units.

The data was fitted with the DANSE software SasView. The simplest form factor that allowed to fit all the mixtures at both temperatures was the form factor of a cylinder with an elliptical cross-section and a homogeneous contrast. The scattering length densities for toluene-$D_8$ (5.66 $10^{-6}$ $Å^{-2}$) and for the low molar mass bis-urea **M** (6.78 $10^{-7}$ $Å^{-2}$) were calculated from the atomic bound coherent scattering lengths. The other samples contained the polymeric bis-urea $\mathbf{X_{PIB}}$, so that the cylinder can be considered to contain a significant amount of solvent. Therefore, the scattering length density for all the mixtures containing $\mathbf{X_{PIB}}$ was adjusted during the simultaneous fit of all the data. The common value that allowed to fit all the systems was 2.00 $10^{-6}$ $Å^{-2}$. Three parameters were adjusted for each sample: the length of the cylinder and the minor and major radii of the elliptical cross-section.

**Differential scanning calorimetry.** Solution-phase differential scanning calorimetry measurements were performed on a high sensitivity TA Instruments nDSC III system (baseline noise ± 15 nW). The sample cell (0.3mL) was filled with the bis-urea solution and the reference

cell with the corresponding solvent. The capillary cells were not capped, and a constant pressure of 5 $10^5$ Pa was applied. The solutions (2 g/L), were analyzed between 10 and 80 °C, using 3 full heating/cooling cycles, at 1 °C $min^{-1}$. The transition temperature, T**, was measured from the second heating scan.

**Fourier Transform Infrared Spectroscopy.** Solution spectra were measured on a Nicolet iS10 spectrometer in KBr cells of 1.0 mm pathlength and are corrected for air, solvent and cell absorption.

**Isothermal titration calorimetry.** Data were recorded on a Microcal VP-ITC calorimeter, injecting a 0.05 mM toluene solution of **M** into 0.05 mM toluene solutions of $\mathbf{M_{PIB}}$ or $\mathbf{X_{PIB}}$. Injections of 10 $\mu$L over 20 seconds were performed every 600 seconds at a stirring rate of 260 rpm.

## Results and Discussion

**Comparison of the stickers**. Bis-urea **T** (Figure 1) was shown to self-assemble by hydrogen bonding into two distinct supramolecular structures of high molar masses. In toluene both structures are in competition, and it is possible to switch the assembly from one structure to the other by changing the temperature.[32] The high temperature structure is a long filament with a single bis-urea in the cross-section,[33] that is responsible for the formation of viscous solutions. The low-temperature structure is a very long and rigid tube with three bis-ureas in the cross-section, that forms viscoelastic solutions (see Figure 2a for a schematic representation).[34] Bis-ureas **X** and **M** self-assemble into the same supramolecular structures, but their relative stabilities are strongly affected by the substitution on the aromatic spacer. The presence of the methyl groups in positions 4 and 6 stabilizes the tube form of **X** because the repulsion between the

methyl and carbonyl groups enforces a noncoplanar conformation of the urea and phenyl moieties and better preorganizes the monomer for hydrogen bonding in the tube structure.[30] In contrast, the additional presence of a methyl group in position 2 destabilizes the tube form of **M** because this methyl group is placed within the tube cavity, where it competes with the entry of solvent molecules.[27] As a consequence, at 10 mM in toluene, the tube structure is stable up to 43°C for bis-urea with tolyl spacer (**T**),[32] up to 110°C for bis-urea with xylyl spacer (**X**)[30] and only below -5°C for bis-urea with mesityl spacer (**M**),[27] so that at room temperature both **T** and **X** form viscoelastic solutions but not **M** (Figure 1). Mixing bis-ureas **T** and **M** significantly improves the stability of the viscoelastic solution (up to 73°C at 10 mM in toluene),[27] which shows that the tubes with a mixed composition are considerably more stable than any of the pure tubes. This synergistic effect was attributed to the enhanced preorganization of bis-urea **M** and to the wider cavity created by bis-urea **T**: addition of bis-urea **M** to the **T**/**M** mixture is favorable only if its content is low enough, so that the tubular cavity is still large enough to accommodate the solvent molecules.

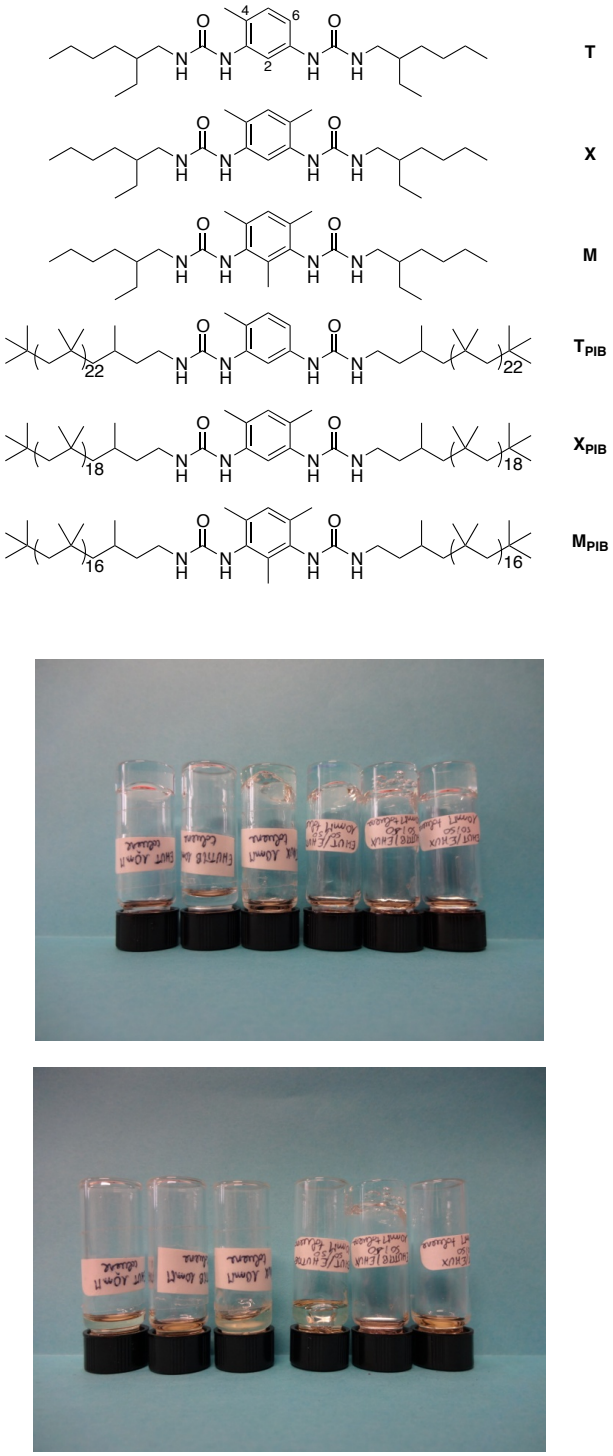


**Figure 1**. Bis-urea structures (top). Appearance of bis-urea solutions and their 1/1 mixtures, at 10 mM (ca 4 g/L) in toluene. From left to right: **T**, **M**, **X**, **T**/**M**, **M**/**X**, **T**/**X** (middle: immediately after turning the vials upside down; bottom: 6 days later).

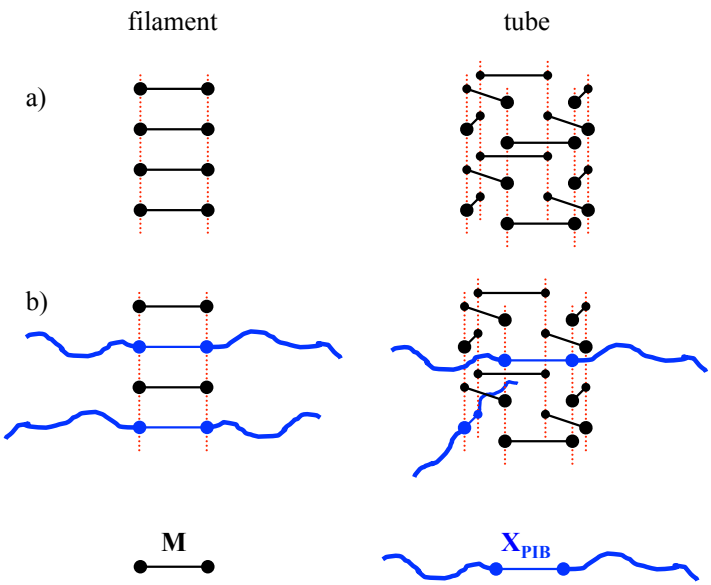


**Figure 2**. a) Schematic supramolecular structures for low molar mass bis-ureas, where the red dotted lines represent the hydrogen bonds between urea groups.[32,33,34] b) Proposed schematic supramolecular structures for the **M**/$\mathbf{X_{PIB}}$ mixtures.

Building on these observations, we first decided to investigate if similar or even stronger synergistic effects could be obtained with the other combinations. Figure 1 shows the appearance of solutions of **T**, **M** and **X** and their equimolar mixtures: although qualitative, this test shows that the composition of the solutions has a strong effect on their flow behavior. The solutions flow in the following order: **M** < **T** < **T**/**X** << **T**/**M** << **X** << **M**/**X**, which means that both **T**/**M** and **M**/**X** mixtures flow more slowly than their pure components, but not the **T**/**X** mixture. This indicates that the presence of the bis-urea with the mesityl spacer (**M**) is essential to obtain a clear-cut synergy, which is in line with the previous explanation that the methyl group in position 2 of the aromatic spacer allows to stabilize the tube assembly, but only if mixed with a less sterically demanding bis-urea. Among the various systems tested, the **M**/**X** mixture forms a particularly strong gel that is worth investigating in detail. However, bis-urea **X** forms metastable

solutions that yield a fine precipitate after several weeks,[35] which complicates structural and thermodynamic studies. Therefore, we considered the bis-ureas made of the same stickers linked to small polyisobutene (PIB) side-chains in the hope that the PIB chains would improve the solubility in non-polar solvents: bis-ureas $\mathbf{T_{PIB}}$, $\mathbf{M_{PIB}}$ and $\mathbf{X_{PIB}}$ (Figure 1) are indeed perfectly soluble in toluene. Table S2 summarizes the appearance of the mixtures combining any low molar mass bis-urea (**T**, **M** or **X**) to any polymeric bis-urea ($\mathbf{T_{PIB}}$, $\mathbf{M_{PIB}}$ or $\mathbf{X_{PIB}}$). This table shows that $\mathbf{M/T_{PIB}}$ and $\mathbf{M/X_{PIB}}$ are systems of interest since they form gels, unlike their pure components. Some of the other mixtures may also be of interest, but the effect may be hidden by the fact that bis-ureas **T** and **X** already form a gel in these conditions.

Therefore, infrared spectroscopy was used to discriminate more sensitively the systems of interest, because the shape of the N-H vibration band is known to be a characteristic signature for the filament and tube structures.[32] Figure 3 shows the relevant part of the spectra for the $\mathbf{M/X_{PIB}}$ mixture. The three spectra show two bands at 3330 and 3270$cm^{-1}$ that are due to hydrogen bonded N-H urea groups (aliphatic N-H and aromatic N-H, respectively). The broadness of these bands for **M** and $\mathbf{X_{PIB}}$ is characteristic for the filament structure, whereas the narrower bands in the case of their mixture is characteristic for the tube structure.[27,32] Therefore, the nature of the assemblies can be estimated from the ratio of absorbances between the maximum (at 3330$cm^{-1}$) and the minimum (at 3300$cm^{-1}$). From the data on Figure 3, it is clear that the $\mathbf{M/X_{PIB}}$ and $\mathbf{M/T_{PIB}}$ mixtures form synergistic co-assemblies because their $A_{max}/A_{min}$ ratio is larger than for both pure components. The effect is less obvious, but may also be present in the case of $\mathbf{T/X_{PIB}}$, $\mathbf{T/M_{PIB}}$, $\mathbf{X/T_{PIB}}$, $\mathbf{X/X_{PIB}}$ and $\mathbf{X/M_{PIB}}$ mixtures for which the $A_{max}/A_{min}$ ratio is larger than the average values of the pure components, meaning that the component that forms the tube structure on its

own (**T** or **X**), converts at least part of the other component ($\mathbf{T_{PIB}}$, $\mathbf{X_{PIB}}$ or $\mathbf{M_{PIB}}$) from the filament to the tube structure.

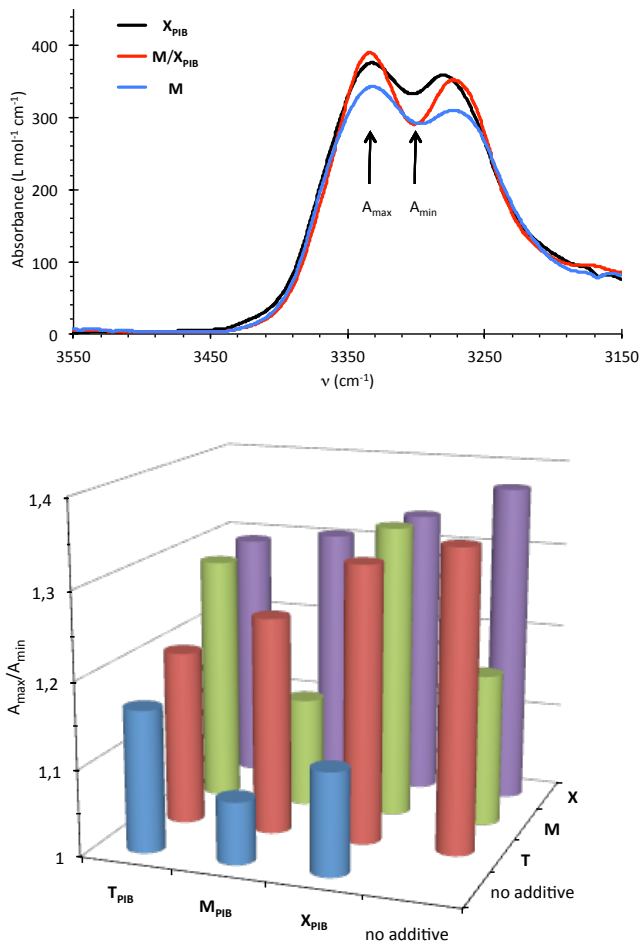


**Figure 3**. Top: FTIR spectra for solutions of **M**, $\mathbf{X_{PIB}}$ and their 1/1 mixture in toluene (5 mM, 25°C) showing the different structure for the mixture. Bottom: ratio of FTIR bands ($A_{max}/A_{min}$) for mixtures in toluene (5 mM). Ratio values $A_{max}/A_{min} \leq 1.2$ (resp. $1.3 \leq A_{max}/A_{min}$) are characteristic for the filament (resp. tube) structure.[32] See Table S3 for the tabulated values.

While all the previous tests were performed with equimolar amounts of both components, it is of interest to see if unbalanced mixtures can also display some synergistic co-assembly. Figure 4 shows capillary viscosity measurements of $\mathbf{T_{PIB}}$, $\mathbf{M_{PIB}}$ or $\mathbf{X_{PIB}}$ solutions at a fixed concentration

(40 g/L) in which a low amount (less than 10 mol%) of **T**, **M** or **X** was added. In these conditions, only two systems display a strong increase in viscosity ($\mathbf{M/X_{PIB}}$ and $\mathbf{X/X_{PIB}}$), and the former system is the most interesting because the viscosity of the mixture is much larger than the viscosity of both pure components. Therefore, this system was selected for further characterization.

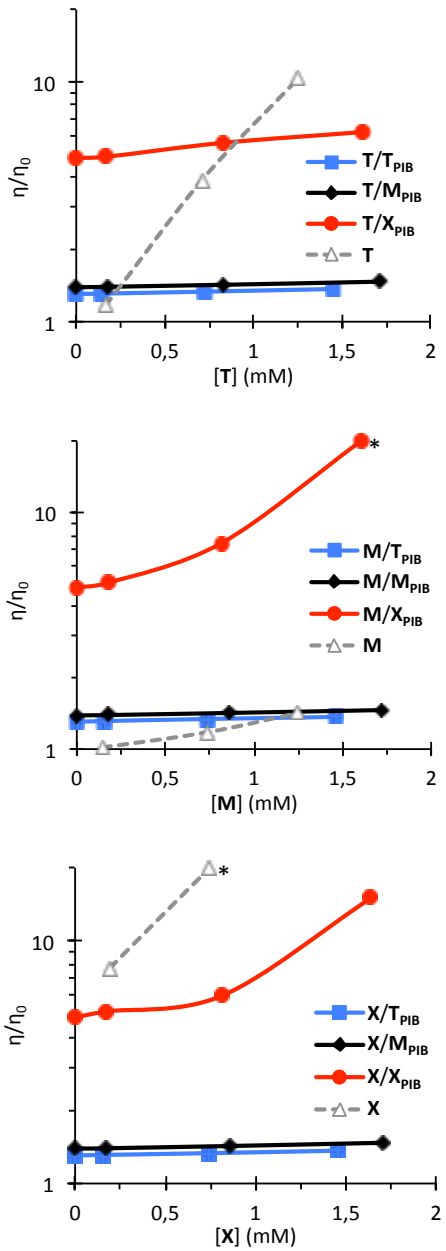

**Figure 4**. Relative viscosity of 40 g/L (16 mM) solutions of $\mathbf{T}_{\mathbf{PIB}}$, $\mathbf{M}_{\mathbf{PIB}}$ or $\mathbf{X}_{\mathbf{PIB}}$ with low amounts of **T** (a), **M** (b) or **X** (c) (toluene, 20°C). The points marked with an asterisk indicate solutions that were too viscous for capillary viscosity measurement.

**Structural and thermodynamic study of the M/$\mathbf{X}_{\mathbf{PIB}}$ mixture.** First of all, the temperature stability of the supramolecular structures was probed by a combination of VT-FTIR spectroscopy and DSC. Figure 5 shows the typical broadening of the FTIR spectra at high temperatures that is characteristic of the transition from the tube to the filament structure (see above). The transition temperature (T** = 70°C) was measured as the mid-point in the plot of the $A_{max}/A_{min}$ ratio. Figure 6 shows the DSC trace obtained for the same system: the transition is detected through an endothermal peak (T** = 68°C, ΔH** = 6.4 kJ/mol). A significant hysteresis is noticed between the heating and cooling curves, but this transition is perfectly reversible, with heating curves that superimpose over at least four heating-cooling cycles. This calorimetric data was obtained for various compositions and is plotted on Figure 6: it shows that the addition of $\mathbf{X}_{\mathbf{PIB}}$ to **M** stabilizes the tube structure by about ΔT** = 75°C.[36] Moreover, the curve has a very broad maximum, which indicates that the optimal composition is close to 1/1, but that deviation from this stoichiometry is not critical. From this calorimetric data, it is also possible to estimate the free energy gain of the M/$\mathbf{X}_{\mathbf{PIB}}$ tube of 1/1 composition compared to the pure **M** tubes through equation 1.[37]

$$\Delta\Delta G = \Delta H^{**}\frac{\Delta T^{**}}{T^{**}} \sim 1\ kJ/mol \quad (1)$$

This value can be compared to the free energy for the formation of such hydrogen bonded supramolecular polymers: in the case of bis-urea **T**, the association constant for the chain

elongation (K) was measured by calorimetry in toluene at 25°C.[30] This association constant is related to the free energy of tube growth through equation 2.

$$\Delta G = -\mathrm{RTlnK} = -34\ kJ/mol \qquad (2)$$

Therefore, the stabilization induced by the complementarity between stickers represents only a small fraction of the overall system.

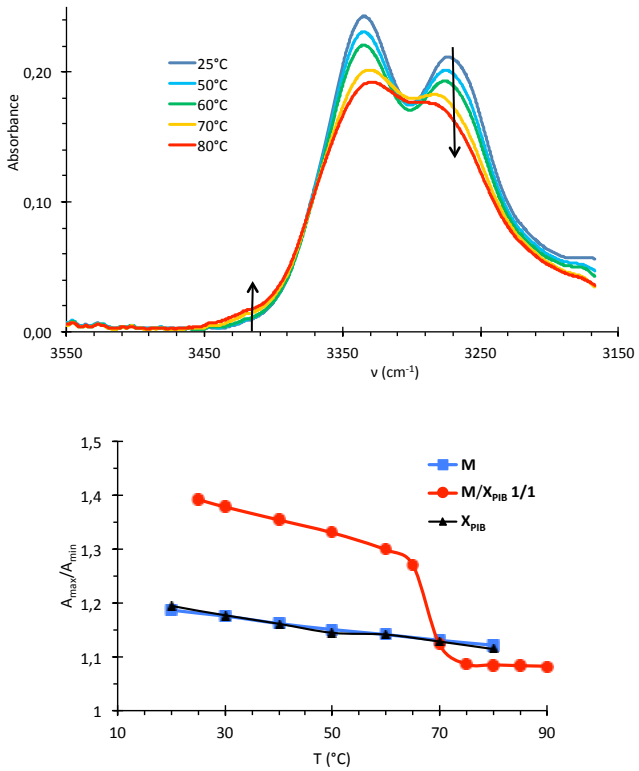


**Figure 5**. Top: FTIR spectra of a **M/X$_{PIB}$** solution at 4g/L in toluene (1/1 molar fraction). Bottom: ratio of FTIR bands ($A_{max}/A_{min}$) versus temperature for the same solution, compared to the pure **M** and **X$_{PIB}$** solutions.

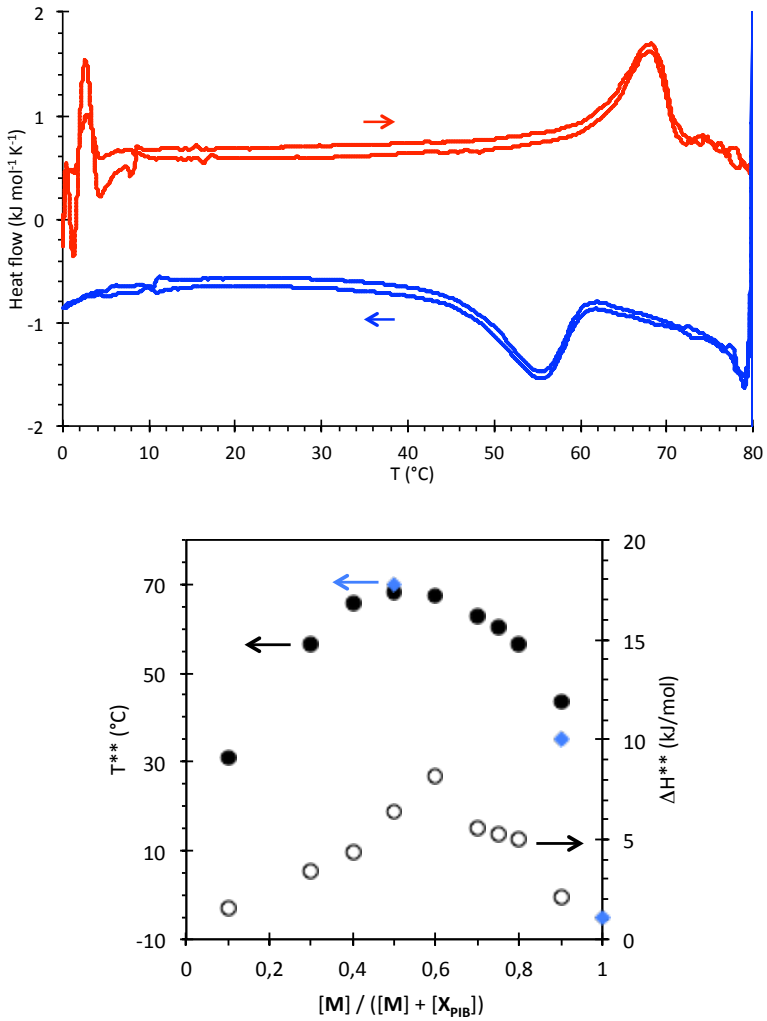


**Figure 6**. Top: DSC thermogram for the **M/X$_{PIB}$** mixture (1/1 molar fraction) in toluene, at a total concentration of 2 g/L. Two cycles of heating and cooling are displayed (1°C/min). Bottom: Transition temperature T** (heating scan) versus composition measured by DSC (black) or FTIR (blue). Hollow points represent the enthalpy of the transition.

The evolution of the transition temperature versus composition (Figure 6) is actually confirmed at the macroscopic level by viscosity measurements (Figure 7) that show a strong increase of viscosity for compositions centered around 1/1. The higher the temperature, the narrower the composition range where a gel is formed, and at 80°C (i.e. above the maximum of T**) no increase in viscosity is detected for the mixtures.

In order to directly evaluate the enthalpic gain of combining **M** and $\mathbf{X_{PIB}}$ molecules, we attempted an Isothermal Titration Calorimetry (ITC) experiment where a solution of **M** in toluene is injected into a solution of $\mathbf{X_{PIB}}$ at the same concentration. The concentration of the experiment had to be lowered to 0.05 mM to reduce the baseline noise due to the viscosity of the solution. Figure 8 shows the corresponding heat flow measured in comparison with a blank experiment where the **M** solution is injected into a $\mathbf{M_{PIB}}$ solution at the same concentration, i.e. where no structural transition is expected because the bis-urea sticker is the same and at the same concentration in the cell and in the syringe. The blank experiment yields comparably small and constant exothermic heat effects that are probably mainly due to the friction during the injections. In contrast the injection of the **M** solution into the $\mathbf{X_{PIB}}$ solution triggers a significant exothermic signal when the composition in the calorimetric cell is rich enough in **M** ($[\mathbf{M}]/([\mathbf{M}]+[\mathbf{X_{PIB}}]) > 0.14$). The magnitude of this exothermic signal is unfortunately difficult to analyze quantitatively because of the continuously increasing viscosity during the experiment, which entails an increasing contribution of the friction. Nevertheless, the result is in good agreement with the data of Figure 6: the addition of **M** to the $\mathbf{X_{PIB}}$ solution produces a significant heat effect only above a critical composition, which probably corresponds to the composition of the filament to tube transition (at 20 °C and 0.05 mM).

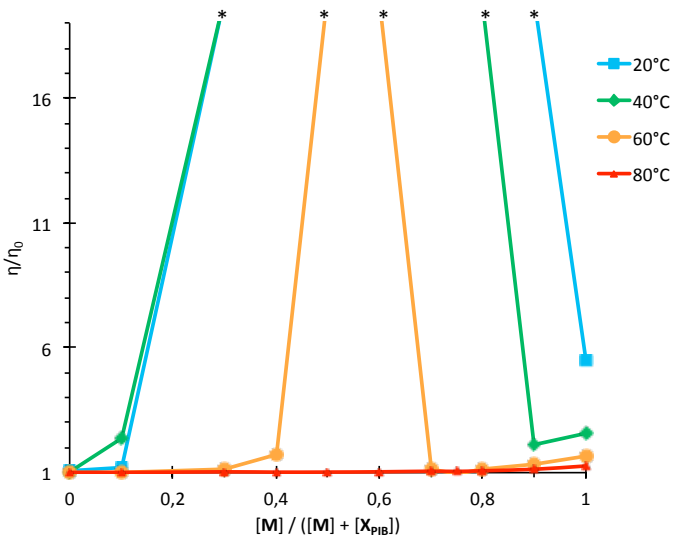


**Figure 7**. Relative viscosity of 2 g/L solutions of **M**/$\mathbf{X_{PIB}}$ in toluene, at various temperatures. The points marked with an asterisk indicate solutions that were too viscous for capillary viscosity measurement.

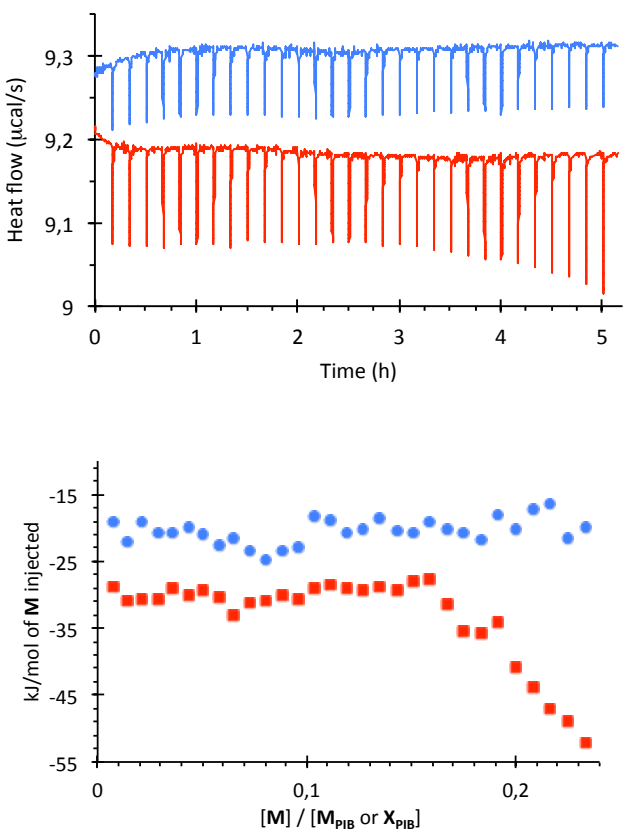

**Figure 8**. ITC data. Top: heat effect produced by injecting 10 μL aliquots of a 0.05 mM solution of **M** in toluene into a 0.05 mM solution of $\mathbf{M_{PIB}}$ (blue) or $\mathbf{X_{PIB}}$ (red) in toluene (T = 20 °C). Bottom: corresponding enthalpograms.

Finally, the structure of the assemblies was probed directly by Small Angle Neutron Scattering (SANS) to confirm our interpretation of the transition between two supramolecular structures. Figure 9 shows the scattered intensity for various $\mathbf{M/X_{PIB}}$ compositions at 20 and at 80 °C. At 20 °C, all curves are characterized at low angles by a $q^{-1}$ dependence of the scattered intensity over one decade. This feature is typical of long and rigid objects. In addition, at larger angles, the systems that contain at least 10% of $\mathbf{X_{PIB}}$ show a $q^{-2}$ dependence of the scattered intensity that is typical of solvated polymer chains. The combination of the $q^{-1}$ dependence at low q and the $q^{-2}$ dependence at large q is a signature for the presence of rod-like objects that are decorated with solvated chains, i.e., hairy rods.[38] Importantly, the fact that the scattered intensity for the mixtures containing 25% or 50% **M** is higher than the intensities for both pure solutions proves that **M** and $\mathbf{X_{PIB}}$ co-assemble into a different and thicker structure than the pure components. Indeed, the scattered intensity in the $q^{-1}$ region depends only on the contrast and on the mass per unit length of the rods. Since the contrast of the mixture is the average of the contrast for the pure components, only a change in mass per unit length of the objects can explain the experimental data.

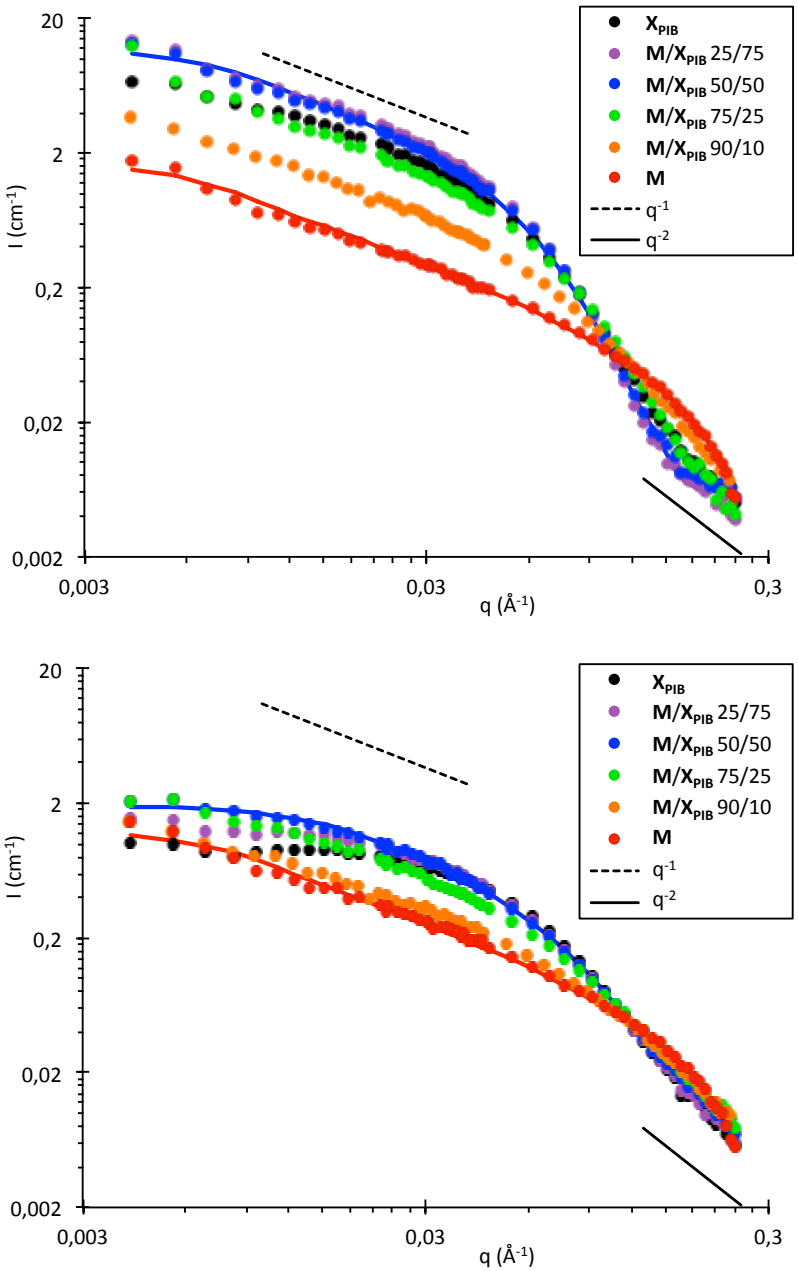


**Figure 9**. SANS intensity (I) versus scattering vector (q) for solutions of **M** or $\mathbf{X_{PIB}}$ at a concentration of 6 g/L in toluene-$d_8$ and for their mixtures (molar fraction). Top: 20 °C. Bottom: 80 °C. The continuous lines are fits according to the form factor of a rod-like cylinder with an elliptical cross-section and homogeneous contrast. See Figures S1 to S6 for the other fits.

At 80 °C, all curves (except for pure **M**) reach a constant intensity at low angles showing that the objects are much shorter than at 20°C.

At the concentration of the experiment (6 g/L), the interactions between objects can be neglected.[29] Therefore, the fit of the data was attempted with various form factors of rigid cylinders. The simplest one that can describe the whole data set is the form factor for a rigid cylinder with an elliptical cross-section and a uniform contrast. Only three parameters were adjusted for each curve: the length of the cylinder and the minor and major radii of the elliptical cross-section. The other parameters (the scattering length densities and the volume fraction) were *a priori* evaluated from the known composition, as explained in the Experimental Section. The fits are displayed on Figures S1 to S6 while the evolution of the geometrical parameters deduced from these fits is shown on Figure 10. At 80°C, both the length of the objects and the dimensions of the cross-section evolve gradually with the composition between those of the pure systems. Therefore, there is no indication of any change in structure with the composition, which is in agreement with the DSC data that showed that 80°C lies above the transition for all compositions. Nevertheless, the addition of the low molar mass bis-urea **M** to the polymeric bis-urea $\mathbf{X_{PIB}}$ induces an increase of the length of the objects, but this is probably simply due to a reduced steric hindrance. In contrast, at 20°C, the cross-section of the objects is larger for some intermediate compositions (25 and 50 mol% of **M**) than for the pure systems. This feature can only be explained if the structure of the assembly at the molecular scale changes with the composition. Following the spectroscopic data discussed above, we propose that all the systems at 80°C and the pure systems at 20°C are assembled into the filament structure that contains a single molecule in the cross-section (Figure 2). In contrast, the 50/50 mixed system at 20°C is assembled into the tube structure that contains three molecules in the cross-section. The

coherence with the SANS data is obvious for the filament structure where the elliptical shape of the cross-section comes from the shape of the monomers. Moreover, the major radius measured for **M** and $\mathbf{X_{PIB}}$ correspond to the respective size of the molecules. At first glance, in the case of the tube structure, one could expect a circular cross-section rather than an elliptical one. However, the presence of two $\mathbf{X_{PIB}}$ molecules at the same level along the tube axis is probably disfavored because of steric repulsion between the PIB chains. Therefore, locally, the cross-section is probably not circular. Of course, at larger length scale the orientations of $\mathbf{X_{PIB}}$ molecules along the tube axis are not expected to be correlated, so that the projection of the assembly along its axis is probably isotropic. For a given composition, the increase in both major and minor radii on lowering the temperature from 80 to 20°C is then probably due to the increased thickness of the structure at the scale of the urea functions (one versus three bis-ureas in the cross-section) and also to a more extended conformation of the PIB chains because of the shorter distances between $\mathbf{X_{PIB}}$ molecules in the tube structure.

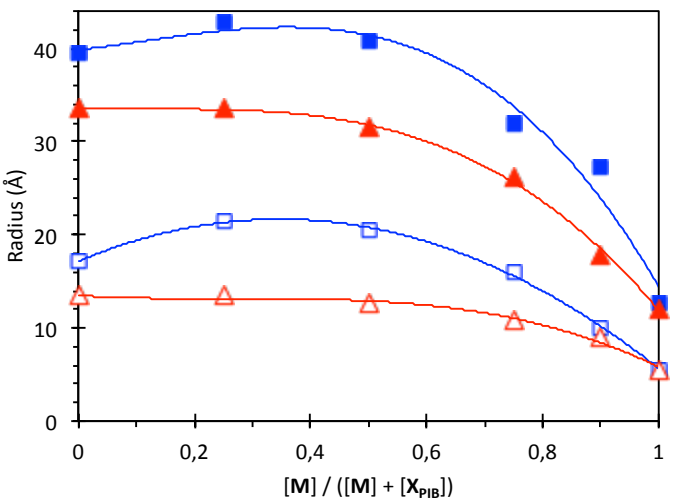

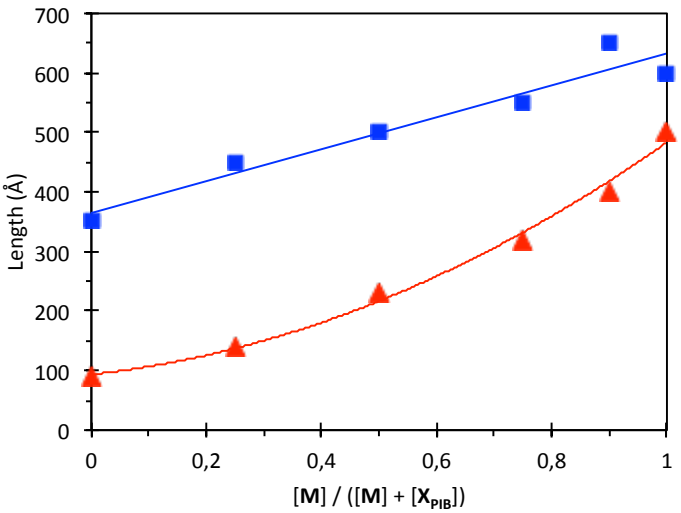


**Figure 10**. Plot of the parameters obtained by fitting the SANS data of Figure 9 with the form factor of a rod-like cylinder with an elliptical cross-section. See Figures S1 to S6 for the fits. Top: major radius (full symbol) and minor radius (hollow symbol) of the cross-section. Bottom: length of the cylinder. Blue: data at 20°C; red: data at 80°C. Note that the transition temperature between the tube and filament structure lies between 20 and 80°C only for the mixtures (see Figure 6).

## Conclusion

Mixing bis-ureas with slightly different structures can yield surprisingly large synergistic effects, as shown here in the case of bis-ureas with an aromatic spacer. A strong increase in viscosity is observed when a bis-urea with the sterically demanding 2,4,6-trimethylbenzene spacer is combined with a bis-urea bearing no methyl group in position 2 of the aromatic spacer (i.e. 4-methylbenzene or 4,6-dimethylbenzene). This effect is the consequence of a change in supramolecular assembly triggered by the composition of the mixture. The mixture of complementary bis-ureas forms rod-like objects that are more stable by about 1 kJ/mol, and that are thicker than the rod-like objects formed by both parent systems.

ASSOCIATED CONTENT

**Supporting Information**. Synthetic procedure and additional FTIR and SANS data.

AUTHOR INFORMATION

**Corresponding Author**

* E-mail: laurent.bouteiller@upmc.fr

ACKNOWLEDGMENT

LLB (Saclay) is acknowledged for providing beamtime for SANS experiments. We thank BASF company for the gift of a Kerocom PIBA sample. This work benefited from DANSE software developed under NSF award DMR-0520547.

REFERENCES

(1) De Greef, T. F. A.; Smulders, M. M. J.; Wolffs, M.; Schenning, A. P. H. J.; Sijbesma, R. P.; Meijer, E. W. Supramolecular Polymerization. *Chem. Rev.* **2009**, *109*, 5687–5754.

(2) Zhao, D.; Moore, J. S. Nucleation-Elongation: A Mechanism for Cooperative Supramolecular Polymerization. *Org. Biomol. Chem.* **2003**, *1*, 3471–3491.

(3) Stupp, S. I.; Palmer, L. C. Supramolecular Chemistry and Self-Assembly in Organic Materials Design. *Chem. Mater.* **2014**, *26*, 507–518.

(4) Weiss, R. G. The Past, Present, and Future of Molecular Gels. What Is the Status of the Field, and Where Is It Going?. *J. Am. Chem. Soc.* **2014**, *136*, 7519–7530.

(5) Ajayaghosh, A.; Praveen, V. K.; Vijayakumar, C. Organogels as Scaffolds for Excitation Energy Transfer and Light Harvesting. *Chem. Soc. Rev.* **2008**, *37*, 109–122.

(6) Elemans, J. A. A. W.; Lei, S.; De Feyter, S. Molecular and Supramolecular Networks on Surfaces: From Two-Dimensional Crystal Engineering to Reactivity. *Angew. Chem. Int. Ed.* **2009**, *48*, 7298–7332.

(7) Lin, N.; Stepanow, S.; Ruben, M.; Barth, J. V. Surface-Confined Supramolecular Coordination Chemistry. *Top. Curr. Chem.* **2009**, *287*, 1–44.

(8) Ciesielski, A.; El Garah, M.; Masiero, S.; Samori, P. Self-Assembly of Natural and Unnatural Nucleobases at Surfaces and Interfaces. *Small* **2016**, *12*, 83–95.

(9) Hosseini, M. W. Self-Assembly and Generation of Complexity. *Chem. Commun.* **2005**, 5825–5829.

(10) Inokuma, Y.; Kawano, M.; Fujita, M. Crystalline Molecular Flasks. *Nat. Chem.* **2011**, *3*, 349–358.

(11) Seoane, B.; Castellanos, S.; Dikhtiarenko, A.; Kapteijn, F.; Gascon, J. Multi-Scale Crystal Engineering of Metal Organic Frameworks. *Coord. Chem. Rev.* **2016**, *307*, 147–187.

(12) Shimizu, L. S.; Salpage, S. R.; Korous, A. A. Functional Materials from Self-Assembled Bis-Urea Macrocycles. *Acc. Chem. Res.* **2014**, *47*, 2116–2127.

(13) Hirst, A. R.; Smith, D. K. Two-Component Gel-Phase Materials - Highly Tunable Self-Assembling Systems. *Chem. - Eur. J.* **2005**, *11*, 5496–5508.

(14) Buerkle, L. E.; Rowan, S. J. Supramolecular Gels Formed from Multi-Component Low Molecular Weight Species. *Chem. Soc. Rev.* **2012**, *41*, 6089–6102.

(15) Lindoy, L. F.; Park, K.-M.; Lee, S. S. Metals, Macrocycles and Molecular Assemblies - Macrocyclic Complexes in Metallo-Supramolecular Chemistry. *Chem. Soc. Rev.* **2013**, *42*, 1713–1727.

(16) Barboiu, M.; Stadler, A.-M.; Lehn, J.-M. Controlled Folding, Motional, and Constitutional Dynamic Processes of Polyheterocyclic Molecular Strands. *Angew. Chem. Int. Ed.* **2016**, *55*, 4130–4154.

(17) Dong, S.; Zheng, B.; Wang, F.; Huang, F. Supramolecular Polymers Constructed from Macrocycle-Based Host-Guest Molecular Recognition Motifs. *Acc. Chem. Res.* **2014**, *47*, 1982–1994.

(18) Chen, G.; Jiang, M. Cyclodextrin-Based Inclusion Complexation Bridging Supramolecular Chemistry and Macromolecular Self-Assembly. *Chem. Soc. Rev.* **2011**, *40*, 2254–2266.

(19) Dastidar, P. Supramolecular Gelling Agents: Can They Be Designed?. *Chem. Soc. Rev.* **2008**, *37*, 2699–2715.

(20) Hardy, J. G.; Hirst, A. R.; Smith, D. K. Exploring Molecular Recognition Pathways in One- and Two-Component Gels Formed by Dendritic Lysine-Based Gelators. *Soft Matter* **2012**, *8*, 3399–3406.

(21) Das, A.; Ghosh, S. Supramolecular Assemblies by Charge-Transfer Interactions between Donor and Acceptor Chromophores. *Angew. Chem. Int. Ed.* **2014**, *53*, 2038–2054.

(22) Ikkanda, B. A.; Iverson, B. L. Exploiting the Interactions of Aromatic Units for Folding and Assembly in Aqueous Environments. *Chem. Commun.* **2016**, *52*, 7752–7759.

(23) Lehn, J.-M. Supramolecular Polymer Chemistry-Scope and Perspectives. *Polym. Int.* **2002**, *51*, 825–839.

(24) Yang, S. K.; Zimmerman, S. C. Hydrogen Bonding Modules for Use in Supramolecular Polymers. *Isr. J. Chem.* **2013**, *53*, 511–520.

(25) Marangoni, T.; Bonifazi, D. Nano- and Microstructuration of Supramolecular Materials Driven by H-Bonded uracil·2,6-Diamidopyridine Complexes. *Nanoscale* **2013**, *5*, 8837–8851.

(26) Elacqua, E.; Lye, D. S.; Weck, M. Engineering Orthogonality in Supramolecular Polymers: From Simple Scaffolds to Complex Materials. *Acc. Chem. Res.* **2014**, *47*, 2405–2416.

(27) Isare, B.; Linares, M.; Lazzaroni, R.; Bouteiller, L. Engineering the Cavity of Self-Assembled Dynamic Nanotubes. *J. Phys. Chem. B* **2009**, *113*, 3360–3364.

(28) Ressouche, E.; Pensec, S.; Isare, B.; Ducouret, G.; Bouteiller, L. Rational Design of Urea-Based Two-Component Organogelators. *ACS Macro Lett.* **2016**, *5*, 244–247.

(29) Lortie, F.; Boileau, S.; Bouteiller, L.; Chassenieux, C.; Deme, B.; Ducouret, G.; Jalabert, M.; Laupretre, F.; Terech, P. Structural and Rheological Study of a Bis-Urea Based Reversible Polymer in an Apolar Solvent. *Langmuir* **2002**, *18*, 7218–7222.

(30) Isare, B.; Pembouong, G.; Boue, F.; Bouteiller, L. Conformational Control of Hydrogen-Bonded Aromatic Bis-Ureas. *Langmuir* **2012**, *28*, 7535–7541.

(31) Pensec, S.; Nouvel, N.; Guilleman, A.; Creton, C.; Boue, F.; Bouteiller, L. Self-Assembly in Solution of a Reversible Comb-Shaped Supramolecular Polymer. *Macromolecules* **2010**, *43*, 2529–2534.

(32) Bouteiller, L.; Colombani, O.; Lortie, F.; Terech, P. Thickness Transition of a Rigid Supramolecular Polymer. *J. Am. Chem. Soc.* **2005**, *127*, 8893–8898.

(33) Brocorens, P.; Linares, M.; Guyard-Duhayon, C.; Guillot, R.; Andrioletti, B.; Suhr, D.; Isare, B.; Lazzaroni, R.; Bouteiller, L. Conformational Plasticity of Hydrogen Bonded Bis-Urea Supramolecular Polymers. *J. Phys. Chem. B* **2013**, *117*, 5379–5386.

(34) Shikata, T.; Nishida, T.; Isare, B.; Linares, M.; Lazzaroni, R.; Bouteiller, L. Structure and Dynamics of a Bisurea-Based Supramolecular Polymer in N-Dodecane. *J. Phys. Chem. B* **2008**, *112*, 8459–8465.

(35) Bis-ureas **T** and **M** form homogeneous solutions in toluene by simply stirring at room temperature, and these solutions are stable for unlimited periods of time. In contrast, bis-urea **X** only dissolves at high temperature and remains optically clear at room temperature for a few weeks only.

(36) Based on FTIR measurement plotted of Figure 6.

(37) Roman, M.; Cannizzo, C.; Pinault, T.; Isare, B.; Andrioletti, B.; van der Schoot, P.; Bouteiller, L. Supramolecular Balance: Using Cooperativity To Amplify Weak Interactions. *J. Am. Chem. Soc.* **2010**, *132*, 16818–16824.

(38) Pedersen, J. S. Form Factors of Block Copolymer Micelles with Spherical, Ellipsoidal and Cylindrical Cores. *J. Appl. Crystallogr.* **2000**, *33*, 637–640.

TOC graphic